Recycling slaughterhouse waste into fertilizer: how do pyrolysis temperature and biomass additions affect phosphorus availability and chemistry?

Marie J. Zwetsloot, Johannes Lehmann[*]*, Dawit Solomon*

Department of Crop and Soil Sciences, Cornell University, NY 14853

[*]Correspondence to: Johannes Lehmann, Bradfield Hall 909, Department of Crop and Soil Sciences, Cornell University, Ithaca, NY 14853. E-mail: CL273@cornell.edu

Abstract

BACKGROUND: Pyrolysis of slaughterhouse waste could promote more sustainable phosphorus (P) usage through the development of alternative P fertilizers. This study investigated how pyrolysis temperature (220, 350, 550 and 750°C), rendering before pyrolysis, and wood or corn biomass additions affect P chemistry in bone char, plant availability, and its potential as P fertilizer.

RESULTS: Linear combination fitting of synchrotron-based X-ray Absorption Near Edge Structure (XANES) spectra demonstrated that higher pyrolysis temperatures decreased the fit with organic P references, but increased the fit with a hydroxyapatite (HA) reference, used as indicator of high calcium phosphate (CaP) crystallinity. The fit to the HA reference increased approximately from 0 to 69% in bone with meat residue and from 20 to 95% in rendered bone. Biomass additions to the bone with meat residue reduced the fit to the HA reference by 83% for wood and 95% for corn, and additions to rendered bone by 37% for wood. No detectable aromatic P forms were generated by pyrolysis. High CaP crystallinity was correlated with low water-extractable P, but high formic acid-extractable P indicative of high plant availability. Bone char supplied available P which was only 24% lower than Triple Superphosphate fertilizer and two- to five-fold higher than rock phosphate.

CONCLUSION: Pyrolysis temperature and biomass additions can be used to design phosphorus fertilizer characteristics of bone char through changing CaP crystallinity that optimize P availability to plants.

Keywords: bone char, biochar, phosphorus, pyrolysis, XANES-spectroscopy

INTRODUCTION

Human impact on the phosphorus (P) cycle has turned rock phosphate into a finite resource as it is more rapidly mined than deposited.[1,2] Despite varying predictions about the depletion time of global P reserves from 50 to 300 years, it is widely accepted that P is a non-renewable resource that requires efficient management.[3,4,5] Fertilizer production utilizes 80-90% of the rock phosphate that is mined annually[5,6] and excessive P fertilizer use has led to pollution of aquatic ecosystems.[7] Hence, making fertilizer production more sustainable is one of the first steps towards a more efficient P cycle and secured agricultural P supply in future.

One proposed solution is to recover P from organic waste disposal[8] and convert it into fertilizer. This option includes producing bone char from slaughterhouse waste by means of pyrolysis, the heating of materials under low oxygen conditions. The European Union has banned the use of bone and meat meal in cattle feed preparation due to the risk of spreading Bovine Spongiform Encephalopathy (BSE).[9] High-temperature pyrolysis may overcome this problem through heat sterilization, as dry heat treatment already at temperatures below pyrolysis temperatures has proven to be an effective method to inactivate BSE prions.[10] Unlike rock phosphate, bone char does not contain toxic metals such as nickel, chrome and cadmium[11,12] making it a less harmful soil amendment.

Calcium phosphates are the primary constituents of bone. Besides the large mineral structure fraction (60%), bone consists of 40% enamel.[13] The bone mineral structure is commonly classified as biological apatite. In comparison to geological apatite such as hydroxyapatite (HA), biological apatite has a smaller crystal size, more carbonate substitutions and a significant OH deficiency, overall resulting in greater solubility.[14,15]

Pyrolysis modifies the chemical and physical structure of bone. Production conditions including pyrolysis temperature significantly alter the yield and quality of bone char.[16] In addition, the meat:bone ratio can drastically change the end product.[17] The thermal

decomposition mainly occurs below 500°C and ends after 750°C.[16,18] With increasing pyrolysis temperature, bone char shows higher calcium phosphate (CaP) crystallinity, smaller ash particle size, fewer carboxyl and amide functional groups, more macro-pores and higher metal concentration in comparison to the original feedstock.[11,12,19] However, the majority of studies about pyrolysis and (co-)gasification of slaughterhouse waste is primarily interested in how production conditions alter its potential as a fuel source[20] and optimize tar production.[21] While there has been an attempt to measure characteristics of the solid product yield,[12] the effect of production parameters on the chemical properties of bone char related to its efficacy as agricultural fertilizer is largely unknown. Although studies have demonstrated the P fertilizer potential of bone char,[22,23,24,25] questions about how pyrolysis temperature and feedstock type change the characteristics of bone char important for the development of effective P fertilizers remain unanswered.

Increasing pyrolysis temperature is assumed to lead to greater P concentrations as shown for animal manures[26,27] and higher CaP crystallinity, suggesting a decrease in solubility.[28] Previous studies have added a carbon source such as coal to the pyrolysis or gasification process of meat and bone meal to prevent stickiness from fatty meat.[9] Co-pyrolyzing bones with a biomass source could also influence CaP crystal formation and may thereby aid in managing P availability to plants. A concurrent production of biochar from biomass could help making P better available to plants,[29,30] but no information about co-pyrolysis of biomass with bones has been published.

Therefore, the objectives of this study were (1) to determine how pyrolysis temperature, rendering bone and mixing bone with a biomass source before pyrolysis affect CaP crystallinity; and (2) to determine the relation between these production conditions and the P fertilizer potential of bone char as represented by P solubility and plant availability indicators. We hypothesized that increasing pyrolysis temperature leads to greater P concentrations but

higher CaP crystallinity, reducing water-soluble P. The addition of biomass prior to pyrolysis was expected to increase CaP crystallinity.

MATERIALS AND METHODS

Material Preparation

Bones with meat residue were collected from Dudley Poultry (Middlesex, NY, USA). Rendered bone meal was purchased from The Espoma Company 1929 (Milville, NJ, USA). Wood chips (80% red maple, 20% sugar maple) were obtained from Robinson Lumber (Owega, NY, USA). Corn stalk and stover came from Cornell Farm Services (Ithaca, NY, USA). Bone with meat residue, wood and corn were oven-dried at 60°C for 5 days and milled to a particle size < 2 mm. An aliquot of 300 g of each material was individually pyrolyzed at a heating rate of 2.5°C min^{-1} and maintained at 220, 350, 550 and 750°C for 45 min in a 9.93 L stainless steel chamber fitted into a muffle furnace. The chamber was swept with argon gas and had rotating paddles for homogenization. In addition, bone with meat residue mixed with wood or corn and rendered bone mixed with wood at a mass ratio of 1:1 were charred under the same pyrolysis conditions. Char yield was measured.

Samples with pyrolysis temperature of 350°C and above were ground with mortar and pestle and sieved to < 74 µm particle size for X-ray Absorption Near Edge Structure (XANES) spectroscopy and to 74-150 µm particle size to control for texture effects on P solubility in the chemical analyses. Bones and biomass samples dried at 60 and 220°C were ground by a Thomas Wiley Mill mesh size 60 (<250 µm) for chemical analyses and processed using a ball grinder for XANES spectroscopy. Possible texture differences of fresh bone or biomass compared to chars may have slightly changed P solubility. To rule out any major effects of specific surface area, a surface analysis using CO_2 (ASAP 2020, Micrometrics Instruments

Corporation, Norcross, GA, USA) was performed on those samples showing the greatest changes in P solubility and extractability. Specific surface area was low and showed a slight decrease from 220°C to 350°C (Supporting Online Table S1).

Rock phosphate (ID, USA) supplied by the Espoma Company 1929 (Milville, NJ, USA) and Greenkeeper's Secret Triple Superphosphate (TSP, T&N, Incorporated, Foristell, MO, USA) were ground to 74-150 µm particle size for chemical analyses.

X-ray Absorption Near Edge Structure (XANES) Spectroscopy

Phosphorus K-edge XANES spectroscopy characterization of the char samples was carried out at beam line X19-A of the National Synchrotron Light Source (NSLS) at Brookhaven National Laboratory (Upton, NY, USA) using a monochromator with Si(111) crystals, photon flux of 5×10^{10} s^{-1} and 2H×1V mm beam spot size. A passivated implanted planar silicon (PIPS)-detector (Canberra Industries, Meriden, CT, USA) measured the P K-edge fluorescence spectra of the samples in a helium-purged chamber. See Sato et al for further details on the beam experimental setup.[31] Samples were mounted in the center of an acrylic sample holder (diameter of 13 mm, depth of 0.5 mm) and covered with a 5-µm thick polycarbonate Mylar X-ray film. Reference P compounds were obtained from a chemical supplier or synthesized as indicated: hydroxyapatite (HA, Sigma Aldrich), synthesized octacalcium phosphate (OCP) which was verified for its chemical characteristics using X-ray powder diffraction analysis, β-tri-calcium phosphate (TCP, Fluka), aluminum phosphate (AP, Fisher Scientific), iron(III)phosphate dihydrate (IPD, Sigma Aldrich), dibasic calcium phosphate (DCP, Sigma Aldrich), dicalcium phosphate dihydrate (DCPD, Riedel de Häen), calcium phosphate monobasic (CPM, Fisher Scientific), sodium phosphate dibasic monohydrate (SPDM, Mallinckrodt Baker Inc.), phytic acid sodium salt hydrate (PASH, Sigma Aldrich), 1-naphthyl phosphate (NP, Sigma Aldrich), diphenyl phosphate (DPP,

Sigma Aldrich) and triphenylphosphine (TPP, Sigma Aldrich). X-ray energy was calibrated to the P K-edge placing the maximum absorption peak of TCP at 2149 eV as reference energy (E0). Single scans of all samples were collected at specific energy ranges: 2134-2144 eV (interval step of 0.5 eV), 2144-64 eV (interval step of 0.1 eV), 2164-2179 eV (interval step of 0.2 eV), 2179-2209 eV (interval step of 1 eV). To increase confidence in results, randomly chosen samples were scanned twice and checked for reproducibility (Supporting Online Figures S1 and S2).

Chemical Analyses

Char, rock phosphate and TSP samples were analyzed for plant-available P with a 2% formic acid extraction at a 1:100 w/v ratio. We did not use the standard AOAC methodology (1M neutral ammonium citrate) to estimate P fertilizer efficacy, since testing with high-ash biochars showed that the 2% formic acid fertilizer extractions had a higher correlation with P uptake by rye-grass (*Lolium multiflorum* Lam.*)* than 1M neutral ammonium citrate or 2% citric acid.[27] This should be taken into consideration when comparing the results of this study to the efficacy of other P fertilizers measured by standard AOAC methods. Orthophosphate content of extracts was analyzed with the ascorbic acid method.[32] As the particle size of the bone char samples was relatively small (74-150 µm), it is important to recognize that fine particles have higher extractability.[33] Water-soluble P, calcium (Ca), magnesium (Mg), potassium (K), iron (Fe), sodium (Na) and sulfur (S) were extracted by shaking char samples in deionized water at a 1:150 solid-solution ratio for 16 h and filtering with 2V Whatman qualitative filter paper.[34] The modified dry-ashing method[35] was used to obtain total P, Ca,Mg, K, Fe, Na and S. Elemental concentrations were quantified in the extracts by inductively coupled plasma atomic emission spectrometry (ICP-AES Thermo Jarrell Ash 166 Trace Analyzer, Thermo Jarrell Ash Corporation, Franklin, MA, USA). To determine pH,

148 samples were shaken in water at 1: 20 solid-solution ratio for 90 minutes and analyzed for pH
149 (Orion 3 Star, Thermo Scientific Inc., Beverly, MA, USA).
150
151 *Data Analysis*
152 The program ATHENA of the IFEFIT software package[36] was used for data processing and
153 analysis of the XANES spectra. After checking the accuracy of the pre- and post-edge
154 parameters of randomly selected scans, spectra were subjected to automatic background
155 correction. Linear combination fitting was performed over the spectral region from 15 eV
156 below to 30 eV above the P absorption edge. To allow for uncertainty, weights of the
157 standards were not fixed to 1. All 13 standards were used in the analysis. A maximum of 4
158 standards were allowed to contribute to a fit. First, the groups of organic, inorganic and CaP
159 standards were separately fitted. Standards that never obtained a weight other than 0 were
160 removed from the analysis. The second round of linear combination fitting used the selected
161 organic, inorganic and CaP standards simultaneously. Fits were compared according to their
162 chi-square values. Fits to the standards were qualitatively interpreted. OCP, a precursor of
163 bone apatite,[37,38] was used as indicator of low CaP bone crystallinity and HA as indicator of
164 high CaP bone crystallinity. In addition, the HA/OCP ratio provided a measure for the
165 degree of bone crystallinity. Lastly, expected curves of the biomass-bone mixtures were
166 calculated arithmetically based on the ratios of total P contents and spectra of the individual
167 materials. They were compared to the measured spectra by plotting them in the same graph.
168 Statistical analyses were performed with software package JMP Pro 10.
169
170

RESULTS AND DISCUSSION

XANES Spectral Features of Standards

CaP standards were selected according to their solubility: CPM > DCPD > DCP > TCP > OCP > HA.[28,39] Except for TPP, the white line energy (absorption edge) fell approximately at 2149 eV (Figure 1) and an oxygen oscillation peak occurred around 2166 eV. The CaP standards, other inorganic standards, and organic P standards were distinctively different from one another. The shoulder around 2151 eV was a unique feature for all CaP standards. This secondary peak sharpened and the absorption edge peak widened for more crystalline CaP references such as HA and OCP, which indicates lower solubility and higher thermodynamic stability.[40,41] For HA, OCP and TCP, a tertiary sharp peak appeared at 2159 eV. CaP standards with a $CaHPO_4$ such as DCP, DCPD and CPM also have a more rounded peak at the same energy range. This observation is in line with the P K-edge XANES spectra of Sato et al.[31] and Ingall et al.[42] but not with the data published by Peak et al.[40] that do not show a tertiary peak at 2159 eV for DCP. This could be attributed to the difference between our sample synthesized by Sigma Aldrich and a natural DCP sample (monetite) used by Peak et al.[40]

IPD was characterized by a pre-absorption edge peak at 2146 eV. AP had a secondary broad peak at 2157 eV. SPDM showed two small peaks in between the absorption edge and oxygen oscillation peak: one similar to the CaP shoulder of more soluble CaP compounds at around 2151 eV and one peak at 2158 eV. The AP spectrum was consistent with other studies, while the post-absorption edge spectrum of IPD was smoother than in other studies.[31,40,42,43]

The main absorption edge peaks of PASH, NP and DDP shifted to the right by 0.2-0.5, which was also reported by Brandes et al.[44] While the shape and width of the absorption edge peak slightly differed among these three organic phosphate standards, they had no other distinctive features. The spectrum of PASH was similar to the scans of other phytic acid species from

196 previous studies.[44,45] The white line energy peak of TPP occurred at 2144.5 eV, which is still
197 in the pre-edge of all other reference compounds. TPP also showed a secondary peak before
198 its major absorption peak at 2142.5 eV. There was no oxygen oscillation peak because TPP
199 was the only compound with no oxygen bound to P. This standard was included to identify P
200 atoms in heterocycles.
201
202 *Phosphorus Chemical Structures in Bone Char*
203 In the case of rendered bone and bone with meat residue, increasing pyrolysis temperature led
204 to widening of the absorption edge peak at 2149 eV, sharpening of the CaP shoulder at 2151
205 eV and the peak characteristic for apatite-like CaP minerals at 2159 eV (Figure 2),
206 demonstrating an increase in CaP crystallinity. This is consistent with results from X-ray
207 diffractrometry.[11] At lower temperatures, the spectra of the OCP standard resembled those of
208 rendered bone and bone with meat residue spectra with a higher degree of fit than HA as
209 shown by Figure 2 and the linear combination fitting results (Table 1). However, with an
210 increase in temperature the P spectral properties of bone with meat residue move from 0 to
211 69% match with HA and those of rendered bone from 20 to 95% match with HA (Table 1). It
212 is important to note that the linear combination fitting results of OCP and HA should not be
213 interpreted quantitatively, but that they can be used to evaluate overall trends. HA used in this
214 study was synthesized and consequently more crystalline than biological apatite. OCP has a
215 similar chemical structure as HA but also contains water in its crystal lattices.[46] As a
216 consequence, disordered and less crystalline bone apatite could show more resemblance to
217 the OCP reference. Therefore, we will interpret a high OCP fit as bone apatite with low
218 crystallinity and a high HA fit as bone apatite with high crystallinity.
219 The rendered bone spectra showed a 37% higher fit with HA than bone with meat residue
220 produced at 750°C, but even at lower temperatures spectra of rendered bone char better

resembled those of the HA reference (Table 1). Rendering removes fatty meat residue, leaving a purer source of CaP mineral showing a higher resemblance with HA even without charring. Moreover, less contamination of fatty meat could facilitate CaP crystal formation at a faster rate during pyrolysis.

Biomass additions reduced CaP crystal formation during bone pyrolysis. At 750°C, corn reduced P resembling HA in bone with meat residue by 95%, and wood decreased HA-type structures in bone with meat residue by 84% and in rendered bone by 28% (Table 1). There are several mechanisms that could explain the reduction of CaP crystal formation. First, the addition of corn or wood biomass resulted in an increase of carbon and organic acids. Adsorption and chemical bonding of these molecules onto CaP crystal surfaces could have blocked sites acting as nuclei for continued crystal growth.[37,47,48] Second, metal ions from the biomass sources could have decreased crystal formation through impeding the growth of nuclei or poisoning the substrate resulting in heterogeneous nucleation.[44] Strong metal inhibitors of CaP crystallization are Cu^{2+}, Zn^{2+} and Mg^{2+},[49,50] none of which were present in high amounts. Cu^{2+}, Zn^{2+} were below the detection limit of the ICP-AES and higher Mg concentration did not correlate with reduced crystal growth (Supporting Online Figure S3 and S4). Future studies should focus on identifying the mechanism responsible for reduced crystal growth.

The organic P standards PASH and DPP constituted a small part of the spectra from bone with meat residue alone and mixed with wood or corn biomass, but not of the spectra from rendered bones and only at low pyrolysis temperatures (Table 1). This indicates that rendering bone removes most organic P being part of the fatty meat residue and that with increasing pyrolysis temperature organic P seems to be broken down and transformed into inorganic P. NP and TPP did not show fits with any of the samples and DPP only matched

with spectra of the original feedstock (Table 1). These results suggest that no heterocyclic P forms were generated through pyrolysis.

Phosphorus Concentration, Solubility and Availability

All samples demonstrated total P enrichment with increasing pyrolysis temperature (Table 2). P vaporization and particulate transfer to air is generally low in comparison to N, S, C and K,[51-54] resulting in a greater P concentration in bone chars produced at higher temperatures. Ca was enriched to a higher degree than P. This increased the molar Ca/P ratio at high pyrolysis temperatures (Table 2). Other studies have obtained a similar relationship between temperature and Ca/P ratio and have found that an increase in Ca/P ratios is coupled with higher HA contents,[55] suggesting higher CaP crystallinity. These results are in line with our XANES data. A threshold at a molar Ca/P ratio of 1.55 seems to divide the bone fertilizers in two groups with higher versus lower CaP crystallinity as represented by HA/OCP ratio (Figure 5.A).

Formic-P (g kg^{-1} total P) also increased with temperature (Table 2), suggesting that bone chars produced at higher pyrolysis temperature provided larger proportions of plant-available P. However, the opposite was true for water-P (g kg^{-1} total P), which decreased with an increase in production temperature (Table 2). Even at lower temperatures, formic-P was substantially higher than water-P (Table 2). The water-soluble P fraction may be an underestimate of the amount of P available for plants, while the formic acid-extractable P fraction may be an overestimate of immediate available P.[56] Overall, amounts of formic-P in bone char reached 147.0±4.7 g kg^{-1}. This P concentration is 5 times greater than in Idaho rock phosphate, 2.5 times greater than in GAFSA rock phosphate[21] and only 24% lower than the formic-P in TSP fertilizer measured as 194.0±4.1 g kg^{-1} (Table 2). It should be recognized that possible changes in particle size may have influenced P extractability[34] with increasing

pyrolysis temperatures, even though a systematic change in size cannot be confirmed and surface area rather decreased.

HA/OCP ratios showed a significant negative correlation with water-P and a significant positive correlation with formic-P (Table 3), resulting in lower water-P and higher formic-P (Figure 5.B). Previous studies confirm that more crystalline CaP such as HA are more stable and, therefore, have lower solubility in water than OCP.[57-59] On the other hand, HA has a higher pH and might be more acid-soluble than other CaP structures. This may explain the increase in formic-P with temperature. As wood and corn additions led to lower crystallinity, water-P increased and formic-P decreased. Rendering slaughterhouse waste prior to pyrolysis led to higher total P and formic-P, but had lower water-P concentration in the chars (Table 2).

CONCLUSION

P K-edge XANES analysis and chemical P extractions showed that pyrolysis temperature increased CaP crystallinity, total P content and formic-P, but decreased P solubility in water. Organic P forms disappeared during pyrolysis in favor of inorganic P forms and no aromatic P was detectable with the methods used in this study. Rendering slaughterhouse waste before pyrolysis resulted in a purer mineral P source with higher total P contents and higher CaP crystallinity. Mixing wood or corn biomass with bone largely reduced CaP crystal formation during pyrolysis. Hence, all three variables – pyrolysis temperature, rendering and biomass addition – can be used to manipulate P characteristics of a bone-based fertilizer that are desirable for a particular farming system. Effects of varying surface area or particle sizes were not specifically investigated, but may have a significant effect on P availability in addition to changes in chemistry. For site-specific application, recommendations would need to recognize the changes in P dissolution and adsorption depending on soil pH. Future

294 research should therefore test a variety of bone chars in diverse cropping systems and soil
295 types to determine which bone fertilizers perform best in different settings.
296

297 **ACKNOWLEDGMENTS**

298 We are grateful for the support by the Towards Sustainability Foundation, CARE-Cornell
299 Impact through Innovations Fund, McKnight Foundation, Bradfield Award, Fulbright and
300 Huygens Talent Scholarship Program. Use of the National Synchrotron Light Source,
301 Brookhaven National Laboratory, was supported by the U.S. Department of Energy, Office of
302 Science, Office of Basic Energy Sciences, under Contract No. DE-AC02-98CH10886. We
303 acknowledge the support by Syed Khalid running beam line X19A.
304

305 **SUPPORTING INFORMATION**

306 XANES spectra of corn and wood chars; formic-P, water-P and total P of commercial
307 fertilizers; formic-P (mg P g^{-1}) of bone-based chars; elemental content of bone-based chars;
308 elemental content of corn and wood chars; water-soluble elements of bone-based chars and
309 corn; duplicates of XANES spectra; specific surface area (SSA) analysis. This material is
310 available free of charge in the online edition of the journal.
311

312 **REFERENCES**

313 1. Neset TSS and Cordell D, Global phosphorus scarcity: identifying synergies for a
314 sustainable future. *J Sci Food Agric* **92:** 2-6 (2012).
315 2. Abelson PH., A potential phosphate crisis. *Science* **283:** 2015 (1999).

316 3. Cordell D, Drangert JO and White S, The story of phosphorus: Global food security and
317 food for thought. *Global Environmental Change* **19:** 292-305 (2009).
318 4. Gilbert N, Environment: The disappearing nutrient. *Nature* **461:** 133-143 (2009).
319 5. van Kauwenbergh SJ, Stewart M and Mikkelsen R, World reserves of phosphate rock… a
320 dynamic and unfolding Story. *Better Crops Plant Food* **97**: 18-20 (2013).
321 6. Smil V, Phosphorus in the environment: Natural flows and human interferences. *Annu Rev*
322 *Energy* **25:** 53-88 (2000).
323 7. Tilman D, Fargione J, Wolff B, D'Antonio C, Dobson A, Howarth R, Schindler D,
324 Schlesinger WH, Simberloff D and Swackhamer D, Forecasting agriculturally driven global
325 environmental change. *Science* **292:** 281-284 (2001).
326 8. Cordell D, Rosemarin A, Schroder JJ, Smit AL, Towards global phosphorus security: A
327 systems framework for phosphorus recovery and reuse options. *Chemosphere* **84:** 747-758
328 (2011).
329 9. Cascarosa E, Gea G and Arauzo J, Thermochemical processing of meat and bone meal: A
330 review. *Renewable Sustainable Energy Rev* **16:** 942-957 (2012).
331 10. Taylor DM, Inactivation of the BSE agent. *J Food Saf* **18**: 265-274 (1998).
332 11. Deydier E, Guilet R, Sarda S and Sharrock P, Physical and chemical characterisation of
333 crude meat and bone meal combustion residue: "waste or raw material?" *J Hazard Mater*
334 **121:** 141-148 (2005).
335 12. Chaala A and Roy C, Recycling of meat and bone meal animal feed by vacuum pyrolysis.
336 *Environ Sci Technol* **37:** 4517-4522 (2003).
337 13. Posner AS, The structure of bone apatite surfaces. *J Biomed Mater Res* **19:** 241-250
338 (1985).
339 14. Wopenka B and Pasteris JD, A mineralogical perspective on the apatite in bone. *Mater*
340 *Sci Eng C* **25:** 131-143 (2005).

341 15. Boskey AL, Mineralization of bones and teeth. *Elements (Chantilly, VA, US.)* **3:** 385-391
342 (2007).
343 16. Ayllon M, Aznar M, Sanchez JL, Gea G and Arauzo J, Influence of temperature and
344 heating rate on the fixed bed pyrolysis of meat and bone meal. *Chem Eng J* **121:** 85-96
345 (2006).
346 17. Cascarosa E; Becker J, Ferrante L, Briens C, Berruti F and Arauzo J, Pyrolysis of meat-
347 meal and bone-meal blends in a mechanically fluidized reactor. *J Anal Appl Pyrolysis* **91:**
348 359-367 (2011).
349 18. Conesa JA, Fullana A and Font R, Thermal decomposition of meat and bone meal. *J Anal*
350 *Appl Pyrolysis* **70:** 619-630 (2003).
351 19. Novotny EH, Auccaise R, Rodrigues Velloso MH, Correa JC, Higarashi MM,
352 Nascimento Abreu VM, Rocha JD and Kwapinski W, Characterization of phosphate
353 structures in biochar from swine bones. *Pesqui Agropecu Bras* **47:** 672-676 (2012).
354 20. Cascarosa E, Gasco L, Garcia G, Gea G and Arauzo J, Meat and bone meal and coal co-
355 gasification: environmental advantages. *Resour Conserv Recycl* **59:** 32-37 (2012).
356 21. Fedorowicz EM, Miller SF and Miller BG, Biomass gasification as a means of carcass
357 and specified risk materials disposal and energy production in the beef rendering and
358 meatpacking industries. *Energy Fuels* **21:** 3225-3232 (2007).
359 22. Warren GP, Robinson JS and Someus E., Dissolution of phosphorus from animal bone
360 char in 12 soils. *Nutr Cycling Agroecosyst* **84:** 167-178 (2009).
361 23. Mondini C, Cayuela, ML, Sinicco T, Sanchez-Monedero MA, Bertolone E and Bardi L,
362 Soil application of meat and bone meal. Short-term effects on mineralization dynamics and
363 soil biochemical and microbiological properties. *Soil Biol Biochem* **40:** 462-474 (2008).
364 24. Siebers N and Leinweber P, Bone char: a clean and renewable phosphorus fertilizer with
365 cadmium immobilization capability. *J Environ Qual*, **42**: 405-411 (2013).

366 25. Siebers N, Godlinski F, Leinweber P, The phosphorus fertilizer value of bone char for
367 potatoes, wheat and onions: first results. *Landbauforschung* **62**: 59-64 (2012).
368 26. Azuara M, Kersten SRA and Kootstra AMJ, Recycling phosphorus by fast pyrolysis of
369 pig manure: concentration and extraction of phosphorus combined with formation of value-
370 added pyrolysis products. *Biomass Bioenergy* **49:** 171-180 (2013).
371 27. Wang T, Camps-Arbestain M, Hedley M, and Bishop P, Predicting phosphorus
372 bioavailability from high-ash biochars. *Plant Soil* **357:** 173-187 (2012).
373 28. Jaynes WF, Moore PA and Miller DM, Solubility and ion activity products of calcium
374 phosphate minerals. *J Environ Qual* **28:** 530-536 (1999).
375 29. Cui HJ, Wang MK, Fu ML and Ci E., Enhancing phosphorus availability in phosphorus-
376 fertilized zones by reducing phosphate adsorbed on ferrihydrite using rice straw-derived
377 biochar. *J Soils Sediments* **11:** 1135-1141 (2011).
378 30. Nelson NO, Agudelo SC, Yuan WQ and Gan J, Nitrogen and Phosphorus Availability in
379 Biochar-Amended. *Soils Soil Sci* **176:** 218-226 (2011).
380 31. Sato S, Solomon D, Hyland C, Ketterings QM and Lehmann J, Phosphorus speciation in
381 manure and manure-amended soils using XANES spectroscopy. *Environ Sci Technol* **39:**
382 7485-7491 (2005).
383 32. Murphy J and Riley JP, A modified single solution method for determination of
384 phosphate in natural waters. *Anal Chim. Acta* **26:** 31-36 (1962).
385 33. Rajan SSS, Brown MW, Boyes MK and Upsdell MP, Extractable phosphorus to predict
386 agronomic effectivenessof ground and unground phosphate rocks. *Fert Res* **32:** 291-302
387 (1992).
388 34. Hollister, CC, Bisogni JJ and Lehmann J, Ammonium, Nitrate, and Phosphate Sorption to
389 and Solute Leaching from Biochars Prepared from Corn Stover (Zea mays L.) and Oak Wood
390 (Quercus spp.). *J Environ Qual* **42:** 137-144 (2013).

391 35. Enders A and Lehmann J, Comparison of Wet-Digestion and Dry-Ashing Methods for
392 Total Elemental Analysis of Biochar. *Commun. Soil Sci Plant Anal* **43:** 1042-1052 (2012).
393 36. Ravel B and Newville M, ATHENA, ARTEMIS, HEPHAESTUS: data analysis for X-ray
394 absorption spectroscopy using IFEFFIT. *J Synchrotron Radiat* **12:** 537-541 (2005).
395 37. Grossl PR and Inskeep WP, Kinetics of octacalcium phosphate crystal-growth in the
396 presence of organic acids. *Geochim Cosmochim Acta* **56:** 1955-1961 (1992).
397 38. Bodier-Houlle P, Steuer P, Voegel JC and Cuisinier FJG, First experimental evidence for
398 human dentine crystal formation involving conversion of octacalcium phosphate to
399 hydroxyapatite. *Acta Crystallogr, Sect D: Biol Crystallogr* **54:** 1377-1381 (1998).
400 39. Montastruc L, Azzaro-Pantel C, Biscans B, Cabassud M and Domenech S, A
401 thermochemical approach for calcium phosphate precipitation modeling in a pellet reactor. .
402 *Chem Eng J* **94:** 41-50 (2003).
403 40. Peak D, Sims JT, and Sparks DL, Solid-state speciation of natural and alum-amended
404 poultry litter using XANES spectroscopy. *Environ Sci Technol* **36:** 4253-4261 (2002).
405 41. Beauchemin S, Hesterberg D, Chou J, Beauchemin M, Simard RR and Sayers DE,
406 Speciation of phosphorus in phosphorus-enriched agricultural soils using X-ray absorption
407 near-edge structure spectroscopy and chemical fractionation. *J Environ Qual* **32:** 1809-1819
408 (2003).
409 42. Ingall ED, Brandes JA, Diaz JM, de Jonge MD, Paterson D, McNulty I, Elliott WC and
410 Northrup P, Phosphorus K-edge XANES spectroscopy of mineral standards. *J Synchrotron*
411 *Radiat* **18:** 189-197 (2011).
412 43. Franke R and Hormes J, The P K-near edge absorption spectra of phosphates. *Physica B*
413 **216:** 85-95 (1995).

414 44. Brandes JA, Ingall E and Paterson D, Characterization of minerals and organic
415 phosphorus species in marine sediments using soft X-ray fluorescence spectromicroscopy.
416 *Mar Chem* **103:** 250-265 (2007).
417 45. Toor GS, Peak JD and Sims JT, Phosphorus speciation in broiler litter and turkey manure
418 produced from modified diets. *J Environ Qual* **34:** 687-697 (2005).
419 46. Johnsson MSA and Nancollas GH, The role of brushite and octacalcium phosphate in
420 apatite formation. *Crit Rev Oral Biol Med* **3:** 61-82 (1992).
421 47. Alvarez R, Evans LA, Milham PJ and Wilson MA, Effects of humic material on the
422 precipitation of calcium phosphate. *Geoderma* **118:** 245-260 (2004).
423 48. Grossl PR and Inskeep WP, Precipitation of dicalcium phosphate dihydrate in the
424 presence of organic acids. *Soil Sci Soc Am J* **55:** 670-675 (1991).
425 49. Madsen HEL, Influence of foreign metal ions on crystal growth and morphology of
426 brushite (CaHPO4, 2H(2)O) and its transformation to octacalcium phosphate and apatite. *J*
427 *Cryst Growth* **310:** 2602-2612 (2008).
428 50. Martin RI and Brown PW, The effects of magnesium on hydroxyapatite formation in
429 vitro from CaHPO4 and Ca-4(PO_4)(2)O at 37.4 degrees C. *Calcif Tissue Int* **60:** 538-546
430 (1997).
431 51. Raison RJ, Khanna PK and Woods PV, Mechanisms of element transfer to the
432 atmosphere during vegetation fires. *Can J For Res* **15:** 132-140 (1985).
433 52. DeLuca TH, MacKanzie MD and Gundale MJ, Biochar effects on soil nutrient
434 transformation, in *Biochar for Environmental Management: Science and Technology*, ed. by
435 Lehmann J and Joseph S. Earthscan Publications Ltd, London, pp. 251-270 (2009).
436 53. Knudsen JN, Jensen PA and Dam-Johansen K, Transformation and release to the gas
437 phase of Cl, K, and S during combustion of annual biomass. *Energy Fuels* **18:** 1385-1399
438 (2004).

439 54. Huang Y, Dong H, Shang B, Xin H and Zhu Z, Characterization of animal manure and
440 cornstalk ashes as affected by incineration temperature. *Appl Energy* **88:** 947-952 (2011).
441 55. Raynoud S, Champion E, Bernache-Assolant D and Thomas P, Calcium phosphate
442 apatites with variable Ca/P atomic ratio I. Synthesis, characterization and thermal stability of
443 powders. *Biomaterials* **23:** 1065-1072 (2002).
444 56. Ylivainio K, Uusitalo R and Turtola E, Meat bone meal and fox manure as P sources for
445 ryegrass (*Lolium multiflorum*) grown on a limed soil. *Nutr Cycling Agroecosyst* **81:** 267-278
446 (2008).
447 57. Lindsay WL and Moreno EC, Phosphate phase equilibria in soils. *Soil Sci Soc Amer Proc*
448 **24:** 177-182 (1960).
449 58. Moreno EC, Brown WE and Osborn G, Stability of dicalcium phosphate dihydrate in
450 aqueous solutions and solubility of octocalcium phosphate. *Soil Sci Soc Amer Proc* **24:** 99-
451 102 (1960).
452 59. Moreno EC, Gregory TM and Brown WE, Preparation and solubility of hydroxyapatite. *J*
453 *Res Natl Bur Stand, Sect A* **72:** 773 (1968).
454

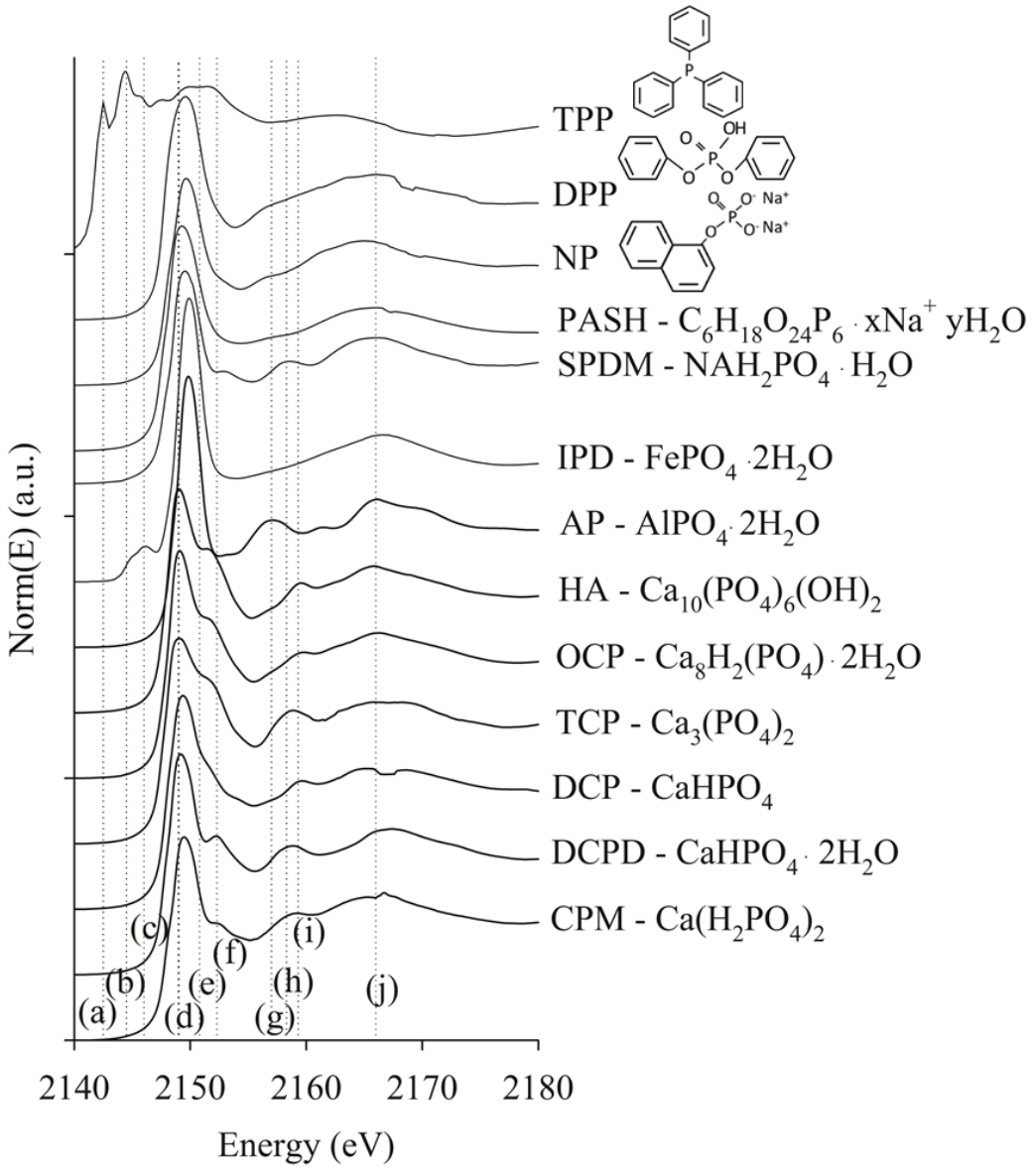

Figure 1. Phosphorus K-edge XANES spectra for P standards species. The dotted lines indicate energy levels that characterize unique spectral features for different P species: (a) triphenylphosphine (TPP), (b) TPP, (c) iron(III)phosphate dehydrate (IPD), (d) absorption edge, (e) octacalcium phosphate (OCP) and hydroxyapatite (HA), (f) calcium phosphate (CaP) species, (g) aluminum phosphate (AP), (h) sodium phosphate dibasic (SPDM), (i) HA and OCP, (j) oxygen oscillation.

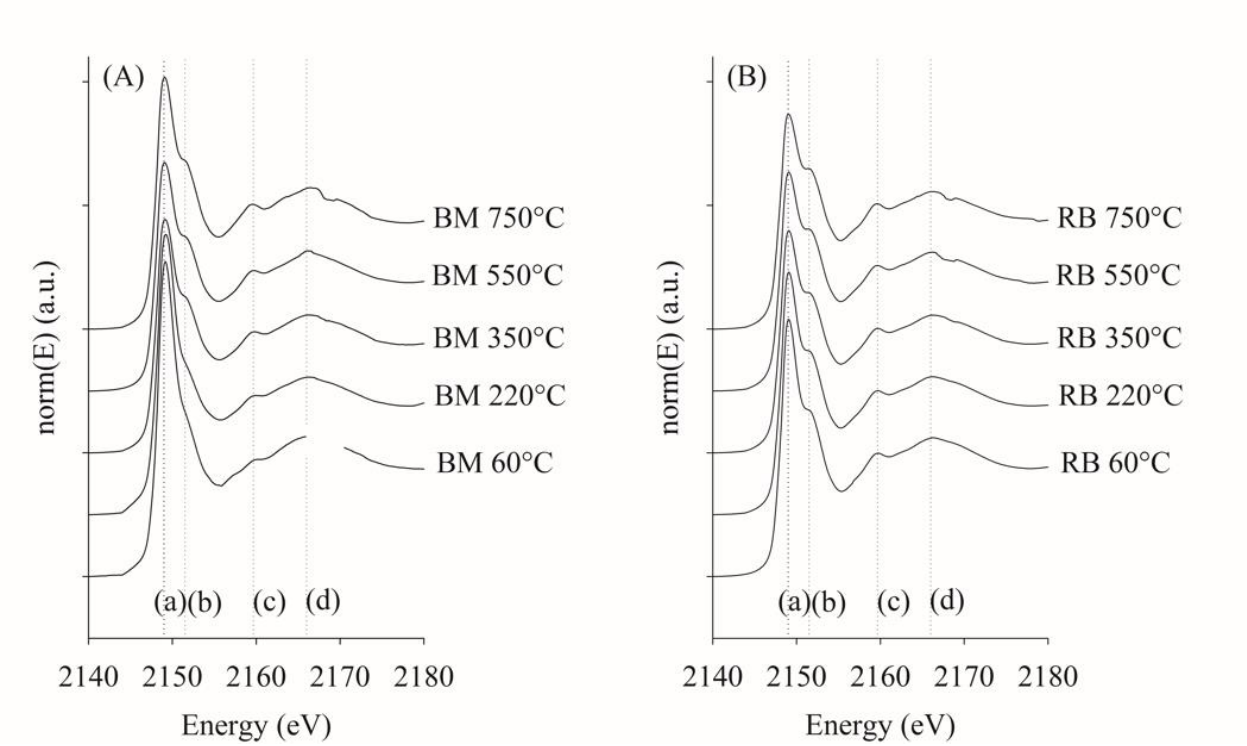

Figure 2. Phosphorus K-edge XANES spectra for bone with meat residue (BM) and rendered bone (RB) at different pyrolysis temperatures. The dotted lines indicate energy levels that characterize unique spectral features for different P species: (a) absorption edge, (b) octacalcium phosphate (OCP) and hydroxyapatite (HA), (c) OCP and HA, (d) oxygen oscillation.

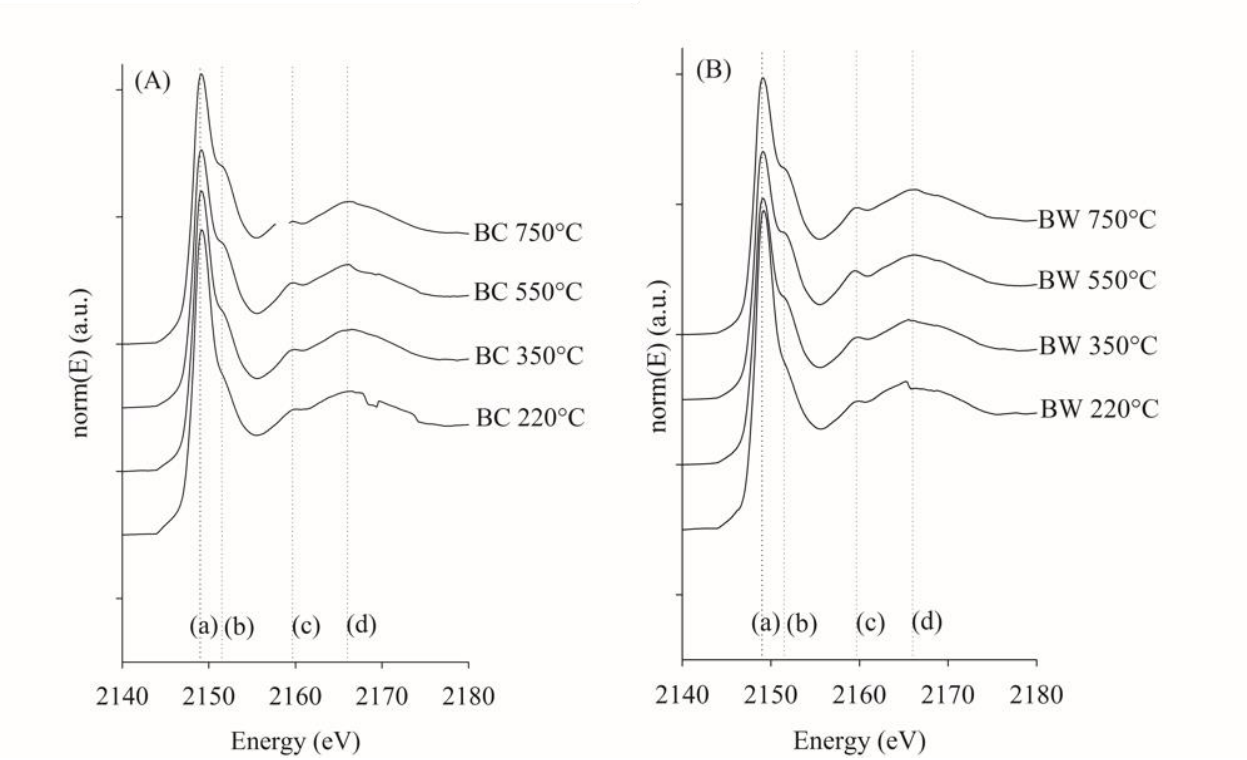

Figure 3. Phosphorus K-edge XANES spectra for mixtures of bone and biomass: (A) bone with meat residue and corn biomass (BC) and (B) bone with meat residue and wood biomass (BW). The vertical dotted lines indicate energy levels that characterize unique spectral features for different P species: (a) absorption edge, (b) octacalcium phosphate (OCP) and hydroxyapatite (HA), (c) OCP and HA, (d) oxygen oscillation.

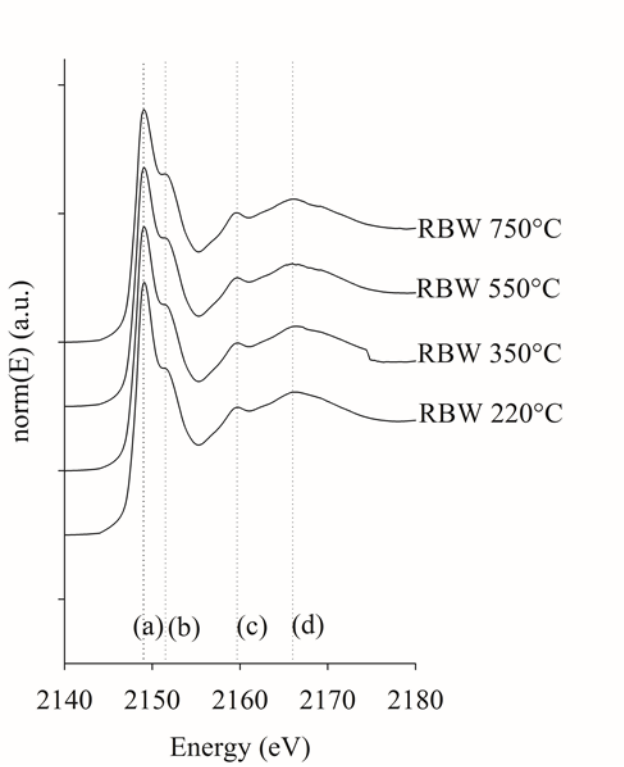

Figure 4. Phosphorus K-edge XANES spectra for mixtures of rendered bone and wood biomass: The vertical dotted lines indicate energy levels that characterize unique spectral features for different P species: (a) absorption edge, (b) octacalcium phosphate (OCP) and hydroxyapatite (HA), (c) OCP and HA, (d) oxygen oscillation.

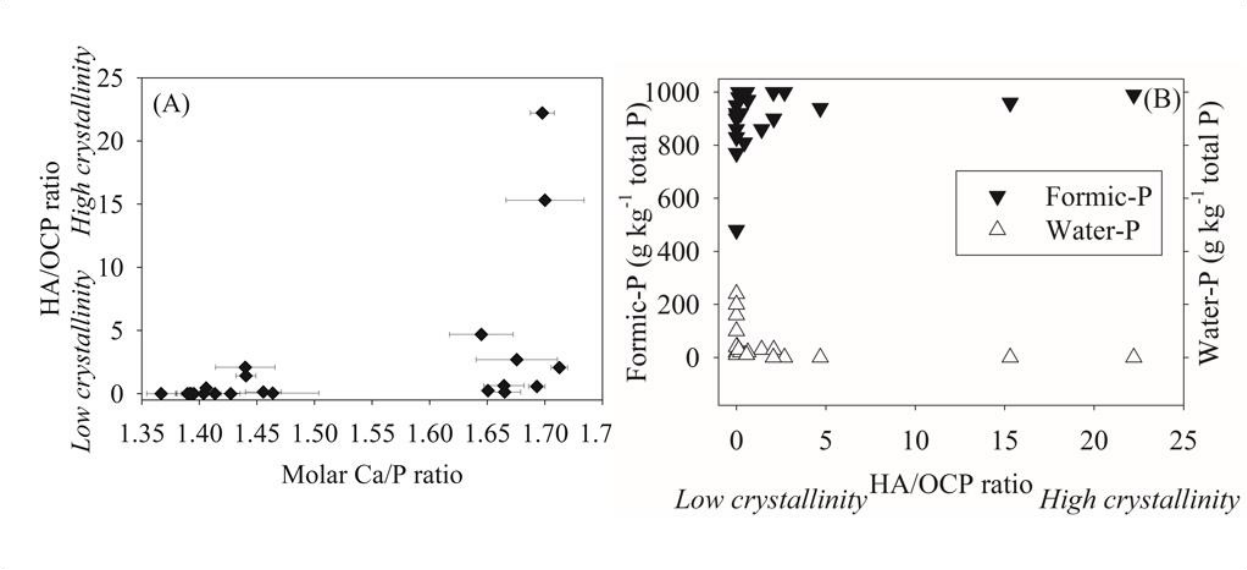

Figure 5. Calcium phosphate (CaP) crystallinity relationships: (A) relation between two indicators of CaP crystallinity molar calcium/phosphorus (Ca/P) ratio and hydroxyapatite/octacalcium phosphate (HA/OCP ratio), (B) effect of HA/OCP ratio as indicator of CaP crystallinity on water-soluble and formic acid extractable P.

Table 1. Linear combination fitting results of different feedstock mixtures dried or pyrolyzed at different temperatures. [a] Feedstock (FS) includes bone with meat residue (BM), rendered bone (RB), bone with meat residue and wood (BW), bone with meat residue and corn (BC), rendered bone and wood (RBW). P species are octacalcium phosphate (OCP), hydroxyapatite (HA), iron(III)phosphate dehydrate (IPD), phytic acid sodium salt hydrate (PASH), diphenyl phosphate (DPP).

FS[a]	T (°C)	OCP (%)	HA (%)	IDP (%)	PASH (%)	DPP (%)	χ^2
BM	60	71.9		15.9	22.6		7.09
BM	220	59.2		11.3	36.4		3.13
BM	350	63.1	27.9	2.8	9		0.38
BM	550	38.1	53.7		9.7		0.30
BM	750	33.2	69.3	3.7			1.26
RB	60	83.4	19.7	2.1			1.27
RB	220	61.7	39.1	2.6			0.54
RB	350	17.3	81.1	3.1			0.07
RB	550	4.2	93.3	4.2			0.07
RB	750	6.2	94.9				0.05
BW	220	67.3		12.1	8.2	23.1	5.13
BW	350	90.7		1.3		12.7	1.14
BW	550	96.9		0.4		6.2	0.71
BW	750	89.2	11.6	1.9			0.36
BC	220	60.7		11.2	37.6		4.41
BC	350	83.2		7.6	14.6		2.46
BC	550	99.1		5.3			0.88
BC	750	100	3.8	4.3			2.01
RBW	220	88.8	11.3	2.5			0.59
RBW	350	64.1	36.5	1.5			0.44
RBW	550	26.9	72.3	3			0.26
RBW	750	33.2	68.5				0.16

Table 2. Chemical Characteristics of Sample: pH, total P, total Ca, formic-P by unit mass and total P, and water-P (means and standard deviation; n=3). [a] Feedstock (FS) include bone with meat residue (BM), rendered bone (RB), bone with meat residue and wood biomass (BW), bone with meat residue and corn biomass (BC), rendered bone and wood biomass (RBW), rock phosphate (RP), and Triple Superphosphate (TSP) fertilizer. [b] Formic-P and water-P are expressed in g kg^{-1} total P. [c] Mass yield of RB at 220°C was not recorded. [d] Nutrient characteristics of these samples were calculated as an arithmetic mean from the two materials it was composed of and pH content was not measured. [e] No standard deviation detected (ND).

FS[a]	T (°C)	pH	Total-Ca (g Ca kg^{-1})	Total-P (g P kg^{-1} char)	Formic-P (g P kg^{-1} char)	Formic-P (g kg^{-1} P)[b]	Water-P (g kg^{-1} P)[b]	Mass yield (% initial)
BM	60	6.3 ± 0.0	58.7 ± 6.9	32.6 ± 3.6	28.1±3.1	861 ± 96	156 ± 15	100
BM	220	6.7 ± 0.0	57.3 ± 3.3	31.3 ± 1.6	15.0±3.1	480 ± 100	102 ± 6	90
BM	350	8.4 ± 0.8	151.7 ± 6.5	83.4 ± 3.6	67.5±3.0	810 ± 36	12 ± 1	38
BM	550	10.6 ± 0.0	194.1 ± 3.2	104.1 ± 1.4	89.8±0.9	862 ± 09	29 ± 1	25
BM	750	11.0 ± 0.0	204.1 ± 5.7	109.5 ± 0.3	98.1±1.9	895 ± 18	30 ± 1	26
RB	60	7.3 ± 0.0	183.4 ± 10.5	85.9 ± 4.7	79.1±2.5	922 ± 29	20 ± 2	100
RB[c]	220	6.8 ± 0.0	189.4 ± 6.0	87.9 ± 0.4	85.0±4.0	967 ± 45	20 ± 1	-
RB	350	7.5 ± 0.0	270.6 ± 7.2	127.1 ± 1.3	119.6±7.0	941 ± 55	3 ± ND[e]	68
RB	550	9.2 ± 0.1	307.2 ± 5.4	139.9 ± 4.4	138.2±1.4	988 ± 10	5 ± ND[e]	60
RB	750	10.2 ± 0.1	337.1 ± 8.2	153.2 ± 2.2	147.0±4.7	959 ± 30	3 ± ND[e]	54
BW[d]	60	-	29.9 ± 3.4	16.3 ± 1.8	14.1±1.6	861 ± 96	156 ± 15	100
BW	220	6.5 ± 0.0	27.8 ±1.5	15.4 ± 0.9	14.7±1.2	951 ± 79	203 ± 10	94
BW	350	8.3 ± 0.1	72.1 ± 2.7	39.7 ± 1.0	30.6±2.1	770 ± 53	15 ± 1	39
BW	550	10.1 ± 0.1	95.4 ± 3.7	53.1 ± 2.5	45.7±2.9	861 ± 54	37 ± 3	30
BW	750	10.5 ± 0.0	106.3 ± 5.1	56.4 ± 1.5	55.1±3.5	977 ± 63	27 ± 2	28
BC[d]	60	-	30.4 ± 3.4	16.6 ± 1.8	14.2±1.6	855 ± 95	163 ± 15	100
BC	220	6.7 ± 0.0	25.4 ± 1.5	14.3 ± 0.6	13.2±1.3	920 ± 88	240 ± 10	101
BC	350	9.6 ± 0.1	69.8 ± 2.4	37.8 ± 1.6	31.3±1.1	829 ± 30	18 ± 1	6
BC	550	10.3 ± 0.0	100.6 ± 2.0	55.7 ± 1.7	50.2±0.3	901 ± 06	44 ± 2	23
BC	750	10.4 ± 0.0	110.1 ± 2.7	58.1 ± 1.0	53.1±2.7	913 ± 47	43 ± 2	17

RBW[d]	60	-	92.3 ± 5.3	43.0 ± 2.3	39.6±1.2	922 ± 29	20 ± 2	100
RBW	220	6.6 ± 0.0	102.1 ± 5.3	47.4 ± 1.6	47.8±0.6	1010 ± 13	34 ± 1	91
RBW	350	7.2 ± 0.1	224.4 ± 4.2	102.4 ± 1.7	102.1±3.4	997 ± 33	6 ± 1	51
RBW	550	8.8 ± 0.0	218.7 ± 3.7	100.9 ± 3.8	101.9±2.9	1010 ± 29	5 ± ND[e]	44
RBW	750	10.1 ± 0.0	258.3 ± 4.5	116.6 ± 2.6	119.0±5.1	1021 ± 44	4 ± ND[e]	41
RP	-	6.6 ± 0.0	224.0 ± 4.2	84.8 ± 1.4	23.7±0.5	279 ± 6	4 ± 1	
TSP	-	3.2 ± ND[e]	161.0 ± 5.2	205.3 ± 1.8	194.0±4.1	945 ± 20	100 ± ND[e]	

Table 3. Spearman's correlations of hydroxyapatite/octacalcium phosphate (HA/OCP) ratio as indicator of calcium phosphate (CaP) crystallinity, formic-P (% of total-P), water-P (% of total-P), pH and pyrolysis temperature.

Variable	By variable	Spearman's ρ	Prob > |ρ|
HA/OCP	Formic-P	0.55	0.008
HA/OCP	Water-P	-0.77	< 0.0001
HA/OCP	pH	0.48	0.024
Temperature	HA/OCP	0.45	0.037
Temperature	Formic-P	0.19	0.403
Temperature	Water-P	-0.34	0.116